



Clustering of carboxylated magnetite nanoparticles through polyethylenimine: Covalent versus electrostatic approach



Ildikó Y. Tóth^{a,*}, Dániel Nesztor^a, Levente Novák^b, Erzsébet Illés^a, Márta Szekeres^a, Tamás Szabó^a, Etelka Tombácza^a

^a Department of Physical Chemistry and Materials Science, University of Szeged, Aradi vt. square 1, Szeged, Hungary

^b Department of Colloid and Environmental Chemistry, University of Debrecen, Egyetem square 1, Debrecen, Hungary

ARTICLE INFO

Keywords:

Magnetite nanoparticles
Carboxylated MNPs
Electrostatic self-assembly
Chemically bonded cluster
Magnetic hyperthermia
MRI contrast agent

ABSTRACT

Carboxylated magnetite nanoparticles (MNPs) are frequently used to develop materials with enhanced properties for MRI and hyperthermia. The controlled clustering of MNPs via covalent or electrostatic approaches provides opportunity to prepare high quality materials. MNPs were prepared by co-precipitation and coated by poly(acrylic acid-co-maleic acid) (PAM@MNP). The clusters were synthesized from purified PAM@MNPs and polyethylenimine (PEI) solution via electrostatic interaction and covalent bond formation (ES-cluster and CB-cluster, respectively). The electrostatic adhesion ($-\text{NH}_3^+$ and $-\text{COO}^-$) and the formed amide bond were confirmed by ATR-FTIR. The averaged area of CB-clusters was about twice as large as that of ES-cluster, based on TEM. The SAXS results showed that the surface of MNPs was smooth and the nanoparticles were close packed in both clusters. The pH-dependent aggregation state and zeta potential of clusters were characterized by DLS and electrophoresis measurements, the clusters were colloidally stable at $\text{pH} > 5$. In hyperthermia experiments, the values of SAR were about two times larger for the chemically bonded cluster. The MRI studies showed exceptionally high transversion relaxivities, the r_2 values are $457 \text{ mM}^{-1} \text{ s}^{-1}$ and $691 \text{ mM}^{-1} \text{ s}^{-1}$ for ES-cluster and CB-cluster, respectively. Based on these results, the chemically clustered product shows greater potential for feasible biomedical applications.

1. Introduction

The biomedical application of magnetic nanomaterials has been in the focus of scientific interest over the past few decades. Magnetite (and partially maghemite) nanoparticles (MNPs) are one of the most promising candidates for this purpose. These superparamagnetic iron oxide nanoparticles (SPIONs) are planned to be used in diagnostics (e.g., contrast agent for magnetic resonance imaging (MRI), magnetic particle imaging) and in different therapies (e.g., targeted drug delivery and magnetic hyperthermia) as well [1–11]. Nevertheless, the most progressive trend is the so-called theranostic approach, i.e., the combination of diagnostics and therapy to get more efficient clinical applications [11–14].

The SPIONs used for these purposes must fulfill a number of criteria, including the MNPs have to be non-toxic, chemically stable, uniform in size and should be well-dispersed in the relevant media. This latter means that the colloidal stability of magnetite nanoparticles is of crucial importance under physiological conditions, for example in blood, in which the pH is ~ 7.3 and the salt concentration is $\sim 150 \text{ mM}$

[1,3,6,7,11,12,15,16]. The naked particles do not meet this criterion, so the MNPs must be coated to prevent their aggregation [16]. There is a wide variety of options for the surface modification of nanoparticles. For example covering the surface of the magnetite NPs by carboxylated polyelectrolytes [17–20] is a very favorable choice (e.g., polyacrylic acid [21], chondroitin-sulfate-A [22], poly(acrylic acid-co-maleic acid) [23], etc.), because this not only provides the necessary colloidal stability of coated nanoparticles, but the free (not bonded) $-\text{COOH}/-\text{COO}^-$ groups are perfect even for binding different drugs (e.g., tissue plasminogen activator [24]).

Many promising SPION products can be found in the literature [11] with the potential of being used in future biomedical applications, but many questions still need to be clarified and for a greater potential in theranostics further enhancement of MNPs is required. One possibility is the preparation of particle clusters. The particle-particle interactions in clusters can modify the magnetic behavior of nanoparticles [25–27], which basically influence their contrast-enhancing effects during MRI diagnostics and heating efficiency during magnetic hyperthermia treatment.

* Corresponding author.

E-mail addresses: Ildiko.Toth@chem.u-szeged.hu (I.Y. Tóth), tombacz@chem.u-szeged.hu (E. Tombácza).

In the past decade the significant advances made in controlled clustering of magnetic nanoparticles have enabled the preparation of high quality nanoparticles with tailored properties (e.g., size, composition) enabling biomedical use [28]. Recently Illés et al. published that clustered oleate double layer (OA) coated MNPs covered by poly(ethylene glycol) showed enhanced MRI contrast compared to the non-clustered nanoparticles [18]. Similar enhancement was realized by Berret et al. [29] in the r_2 relaxivities of MNPs clustered electrostatically via oppositely charged polyions. Nesztor et al. synthesized poly(acrylic acid-co-maleic acid) coated magnetite nanoparticles (PAM@MNP) clustered by branched polyethylenimine (PEI-cluster). These magnetic clusters were prepared via electrostatic adhesion of oppositely charged PEI and PAM@MNP. Two different mixing methods, as well as the effect of PEI's relative amount and electrolyte (NaCl) concentration on the cluster formation were tested to choose the optimal preparation of electrostatically bonded clusters [30]. Friedrich et al. attached tissue plasminogen activator (tPA) proteins to PAM@MNP nanoparticles via electrostatic adsorption and covalent binding strategy using an amino-reactive activated ester reaction. The behavior of these products was particularly different [24]. The covalent binding strategy could also be used in case of the PEI and PAM@MNP particles and the clusters prepared by this reaction should be slightly different from the electrostatically bonded clusters.

The fundamental aim of this work is the preparation and comprehensive characterization of PEI-clusters obtained by electrostatic interaction or chemical bonding of the components. First, we synthesized the magnetite by co-precipitation and after the purification the nanoparticles were coated by PAM. The clusters were prepared from purified PAM@MNP nanoparticles and PEI solutions via electrostatic interaction and chemical bond formation. Then we characterized the clusters by TEM and SAXS, and we studied their pH-dependent surface charging and aggregation properties. Next, we identified the bonds between the PAM@MNP and PEI by FTIR-ATR. Finally, we tested the products in magnetic hyperthermia and in MRI diagnostics.

2. Materials and methods

2.1. Synthesis and materials

2.1.1. Synthesis of MNPs

Magnetic nanoparticles were prepared by co-precipitation method published in our earlier paper [17,31]. $\text{FeCl}_2 \cdot 4\text{H}_2\text{O}$, $\text{FeCl}_3 \cdot 6\text{H}_2\text{O}$ and NaOH were analytical grade and purchased from Molar, Hungary. The purified sol was stored at pH~3 and it was identified as magnetite by X-ray diffraction. The magnetite nanoparticles (MNP) were spherical and their average diameter was ~10 nm based on TEM [22,32].

2.1.2. Synthesis of PAM-coated MNPs

Carboxylated magnetite nanoparticles were prepared by surface modification. Poly(acrylic acid-co-maleic acid) with molecular weight ~1800 Da (PAM, purchased from Sigma-Aldrich) was mixed with MNP sol in a ratio of 1.1 mmol PAM (total amount of carboxylate and carboxylic groups) to 1 g MNP (i.e., mmol/g). The pH was set to ~6.5, and one day was ensured for the adsorption process [23]. The amount of PAM which was not adsorbed on MNPs was completely removed from the sol by an excessive washing process. During this, the pH was set to ~3 which resulted in the aggregation of PAM-coated magnetite nanoparticles (PAM@MNP). The PAM@MNP were settled by a strong magnet and the supernatant was removed, after which the particles were re-dispersed in ultra-pure water. This process was repeated three times. Finally, the pH was set to ~6.5, and the stable sol of PAM@MNP contained approximately 0.9 mmol adsorbed PAM/1 g MNP [23,30]. Due to the presence of $-\text{COOH}$ and $-\text{COO}^-$ functional groups on the surface of PAM@MNP particles, at pH~6.5, the amount of charge on the surface is approximately -0.175 mmol/g based on the potentiometric acid-base titration as published earlier [30].

2.1.3. Preparation of PEI-solution

For the preparation of clusters, branched polyethylenimine with the molecular weight of ~25000 Da (PEI, purchased from Sigma-Aldrich) was used. PEI has three different, N-containing moieties: primary, secondary and tertiary amino groups, which can be protonated at different pH-ranges. At pH~6.5 the positive charge on PEI is derived from the protonated amino groups, and the amount of charge is $+10.30$ mmol/g based on potentiometric acid base titration [30]. As a result of this opposite charge formation the interaction between deprotonated carboxylates (PAM@MNP) and protonated amino groups (PEI) was controlled during the preparation of clusters. The synthesis of clusters was performed in two different ways, i.e., the electrostatic structural self-assembly and the chemical bond formation.

2.1.4. Synthesis of electrostatically bonded PEI-cluster

The "electrostatic way" relies on the extensive charge screening and concomitant loss of repulsive double layer forces upon adsorption of PEI [33,34]. This method is a type of self-assembly. The clusters were prepared by mixing the PEI-solution (5 mL, 56.9 mg/L) and the PAM@MNP sol (5 mL, 20 g/L) adjusted to the same pH and ionic strength (pH~6.5 and 10 mM NaCl). The synthesis was performed by synchronous flow method, i.e., the two precursors were simultaneously and promptly injected into a vial and sonicated for 1 min immediately after mixing [30]. In the prepared clusters (ES-cluster) the PEI to PAM@MNP charge ratio is approximately 0.17. The exact iron content of the sample was determined by inductively coupled plasma (ICP) method using an Optima 7000 DV ICP-OES instrument (Perkin-Elmer, Shelton, CT, USA), thus the magnetite content of the ES-cluster's sol is 9.1 g/L.

2.1.5. Synthesis of chemically bonded PEI-cluster

In case of the novel "chemical way", 1.8 mL MES buffer (192.1 mg MES·H₂O, pH ~6.2, purchased from Sigma-Aldrich) was added to 22 mL PAM@MNP sol (1.75 g/L), the mixing was provided by ultrasonication (US) treatment (impulse mode). During further sonication, 0.35 mL PEI solution (0.1 mg/mL) was dosed into the mixture, then the vessel was put into cold water (~0 °C). Finally, 31.5 mg 1-ethyl-3-(3-dimethylaminopropyl)carbodiimide monohydrochloride (Sigma-Aldrich) was added to the mixture under US treatment. The vessel was stored in refrigerator for 2 days, occasionally shaking and ultrasonication (5 impulses) the sample. The purification was accomplished by dialysis (MWCO=6–8 kDa) against ultra-pure water, the end-point of dialysis was ~5 $\mu\text{S}/\text{cm}$. The sample was let to settle on a magnet for two days, and the supernatant was removed. The prepared clusters (CB-cluster) were dispersed in 5 mL ultra-pure water. The PEI to PAM@MNP charge ratio is approximately 0.06. The exact iron content was determined by ICP as mentioned above, thus the magnetite content of the CB-cluster's sample is 5.3 g/L. It is important to note that according to our previous experience, the use of MES as a buffer agent is strongly recommended for obtaining a suitable degree of functionalization [35].

2.1.6. Materials

NaCl, HCl and NaOH, used to set the pH and ionic strength, were analytical grade products of Molar (Hungary). The majority of experiments were performed at pH=6.5 \pm 0.3 so we simplify the notion of this pH value as ~6.5 and omit to note pH unless it has special significance or the values are different. Ultra-pure water was provided by a Zeener water purification system (HumanCorp, Korea). The experiments were performed at 25 \pm 1 °C.

2.2. Transmission electron microscopy (TEM)

The TEM micrographs of clusters were taken by a JEOL JEM 1400+ transmission electron microscope. The accelerating voltage of 80 kV was applied; the maximum resolution of the instrument is

0.2 nm. One drop of highly diluted sol was dried onto a carbon film coated copper grid. The average size distributions of the magnetite nanoparticles were determined by evaluating ~100 particles using the JMicroVision 1.2.7 software.

2.3. Dynamic light scattering (DLS) measurements

For characterization of pH-dependent aggregation state of nanoparticles and clusters, the average hydrodynamic diameter (*Z-Ave*) of PAM@MNP particles and of different clusters was determined at 25 ± 0.1 °C by dynamic light scattering (DLS) method, using a Nano ZS apparatus (Malvern) with a 4 mW He–Ne laser source ($\lambda=633$ nm) operating in backscattering mode at an angle of 173° . The dispersions were diluted to get an optimal intensity of $\sim 10^5$ counts per second, thus the samples contained approximately 100 mg/L of magnetite. The samples were homogenized in an ultrasonic bath for 10 s prior to the measurements, after which 2 min relaxation was allowed in disposable zeta cells (DTS 1060). Any changes in the aggregation state of the nanoparticles and clusters in aqueous dispersions were characterized by the hydrodynamic diameter (*Z-Ave*). The influence of the PEI and the effect of pH variation (between 3 and 10) were studied in 10 mM NaCl solution. For evaluation, the second- or third-order cumulant fit of the autocorrelation functions were used, depending on the degree of polydispersity.

The salt tolerance of PEI-clusters was studied only by visual observation in 0, 10, 50, 90, 120, 150, 200, 300, 400 and 500 mM NaCl solutions at pH~6.3. The dispersions were photographed after standstill for 3 h, which started after 10 s of sonication. Based on our former experiences, a sample without sedimentation for 3 h is considered to be colloidally stable under the given conditions.

2.4. Electrokinetic potential measurements

The electrophoretic mobility of the PAM-coated magnetite and PEI-cluster dispersions was measured at 25 ± 0.1 °C in the same apparatus used for DLS. The zeta-standard of Malvern (-55 ± 5 mV) was used for calibration. The pH range and the ionic strength were identical to those in the DLS experiments. The Smoluchowski equation was applied to convert electrophoretic mobility to electrokinetic potential value. The accuracy of the measurements was ± 5 mV.

2.5. Small-angle X-ray scattering (SAXS) measurements

Structural investigations of PAM@MNP nanoparticles and PEI-clusters were performed by SAXS measurements using synchrotron radiation at the P12 BioSAXS facility with high brilliance X-ray beam (PETRA III storage ring – EMBL/DESY Hamburg). The beamline is optimized for solution scattering experiments and allows the investigation of water based suspensions of magnetic sols. Before the measurements of the magnetic samples, signal from the background solution was measured by the point-collimation SAXS instrument, and it was used for background subtraction. Data were analyzed by fitting theoretical model suitable to describe the scattering from surface and volume fractals as well as by Porod plot. The magnetic samples contained 1 g/L magnetite, the pH was set to ~6.5 and there was no added NaCl in the samples.

2.6. Attenuated total reflection Fourier transform infrared spectroscopy (ATR-FTIR)

ATR-FTIR spectra were recorded with a Bio-Rad Digilab Division FTS-65A/896 spectrometer (with DTGS detector), using a Harrick's Meridian Split Pea Diamond ATR accessory. The absorbance of the samples was measured in single reflection mode over the $400\text{--}4000$ cm^{-1} range (with resolution of 2 cm^{-1}), accumulating 256 scans. The background spectra were measured on a clean and dry

diamond crystal. The suspensions of PAM@MNP nanoparticles, PEI-clusters as well as the solution of PEI were dried on the diamond crystal surface. The pH of each sample was set to ~6.5 to get the functional groups in comparable protonation / deprotonation states.

2.7. Magnetic hyperthermia

The magnetic hyperthermia efficiency of the samples was tested in a magneThermTM (nanoTherics Ltd., Keele, Staffordshire, UK) instrument. The volume of ES- and CB-clusters dispersions was 4 mL, and the concentrations were 9.1 and 5.3 g/L, respectively. The mode of clusterisation, as well as the resonant frequency (109.5, 329.1, 465.3 and 621.7 kHz, $B=9.146$ mT) and magnetic field (6.173, 9.147, 12.347, 20.578 and 24.694 mT, $f=109.5$ kHz) were studied. The measurement time in the hyperthermia setup was 15 min and the specific absorption rate (SAR, W/g magnetite) values for the initial rate of temperature change were calculated according to the approximating equation $SAR=(c_{p,s}m_{medium}/m_{magnetite})\cdot(\Delta T/\Delta t)$, where $c_{p,s}$ is the specific heat capacity was approximated with that of the medium (water), m_{medium} and $m_{magnetite}$ are the masses of the medium (water) and the magnetite nanoparticles, respectively, and $\Delta T/\Delta t$ is the initial temperature rate calculated in the range of 20–200 s

2.8. Magnetic Resonance Imaging (MRI)

The MRI contrast enhancement efficiency of PAM@MNP nanoparticles, PEI-clusters was studied by determining T_2 (transversal) relaxation times by using a clinical MRI instrument, GE Excite HDxt (GE Medical Systems, Milwaukee, WI) at a magnetic field strength of 1.5 T. The contrast enhancement of the magnetic samples was measured using the standard “birdcage” head coil. The dispersions were prepared at nominal Fe concentrations of 0.009, 0.018, 0.045, 0.09, 0.135, 0.18 and 0.22 mM. After the MRI measurements the exact iron content of the samples was measured again by ICP method mentioned in Section 2.1.4. The plastic vials contained 4 mL of the diluted samples. They were placed in a plastic box filled with water and put in the center of the head coil. The r_2 relaxivities were calculated from the $1/T_2$ vs. Fe concentration plots as described in our previously published paper [18].

3. Results and discussion

3.1. Structural characterization of prepared magnetic clusters

Transmission electron microscopy (TEM) can be used to directly image nanoparticles, thus this method is suitable to determine the average primary particle size of magnetite nanoparticles and the estimated area occupied by the clusters on the grid. The TEM pictures characteristic of the ES- and CB-clusters are shown in Fig. 1. The average size of primary particles is 9.0 $\text{nm} \pm 1.5$ nm for the ES-clusters and 10.3 $\text{nm} \pm 1.9$ nm for the CB-clusters. These values are very close to the average particle sizes of the naked MNPs before the surface modification and clustering process [22,32]. At the same time, comparing the representative TEM images taken at the same magnification (Fig. 1) the average area occupied by the chemically bonded clusters on the grid is about twice as large as that of ES-clusters. It is also important to note that the smaller ES-clusters seem to be more compact than the chemically bonded clusters. Thus the accessibility of water molecules to MNPs in the electrostatically bonded cluster is lower.

This difference is probably explained by the variation in the synthesis conditions. In case of the electrostatically adhered clusters, the preparation was carried out at room temperature with continuous ultrasonication, thus attachment of particles via electrostatic interaction is instantaneous, i.e., electrostatic self-assembly occurs [29]. Therefore, despite the presence of relatively larger amount of PEI in

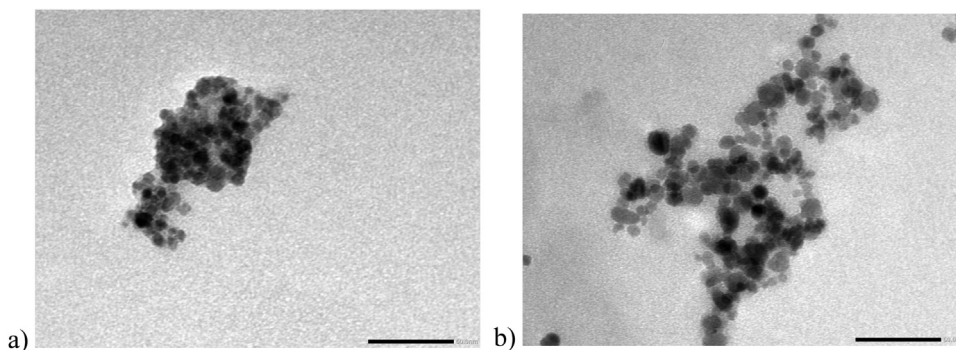


Fig. 1. TEM pictures of a) ES-clusters and b) CB-clusters at the same magnification. The black lines indicate 50 nm.

the system, there is no possibility of formation of large clusters. In contrast, the peptide bond formation was performed at low temperatures without stirring the sample constantly. The chemical reaction is very slow, which provides an opportunity to the formation of larger clusters.

The small-angle X-ray scattering (SAXS) is a useful technique for the structural characterization of nanoparticle systems [36–38]. In the water based sols, the electron density of magnetite is much higher than these values representative for the other components in the samples (e.g., coating polyelectrolyte (PAM) and clustering agent (PEI)), thus information characteristic only of MNPs can be derived by the analysis of the raw data. The SAXS results are shown in Fig. 2 as the double logarithmic plot of I (background subtracted scattering intensity of the sample) and q (scattering vector) [36] and as the Porod plot [38], respectively.

As it is seen in Fig. 2a, the double logarithmic plots ($\log_{10}(I)$ versus $\log_{10}(q)$) yields curves with multiple straight sections. Each isolated straight section was separately fitted with the power law $I=q^{-s}$, where the s parameter refers to the opposite value of the slope. The range of $\log_{10}(q)$ from -1.3 to -0.7 is characteristic of the volumetric properties and the range from -0.3 to 0 is representative of surface structure [36]. The calculated slopes are shown in Table 1.

The theoretical value of volume fractal (s_1) is in the range of 1–3 corresponding to a transition from a chain-like to a space-filling aggregate structure [36]. The calculated s_1 values for our samples are about ~ 2.4 , which resemble a relatively close packing of MNP particles in each sample. Only the chemically bonded cluster's value differs slightly, which is closer to 1 so means less compact system similarly to shown earlier regarding the TEM images.

In case of the surface fractal, the theoretical value $s_2 (=6-d)$ is in the

Table 1

The fitted s parameter from $I=q^{-s}$ equation and calculated surface fractal dimension (d) for the PAM@MNP nanoparticles and PEI-clusters, s_1 is characteristic of the volumetric properties and s_2 is representative of the surface structure ($s_2=6-d$) of the MNPs.

	s_1	s_2	d
PAM@MNP	2.64	3.95	2.05
ES-clusters	2.65	3.91	2.09
CB-clusters	2.26	4.15	1.85

range of 3–4, i.e., surface fractal dimension (d) covers values from 3 to 2, where 3 indicates a rough surface and 2 represents a smooth surface. The calculated s_2 values are about ~ 4 for our sols, thus the surface fractal dimension is about ~ 2 which proves that the magnetite nanoparticles have smooth surface [36]. The Porod plot can be graphed by $\ln(I \cdot q^4)$ versus q^2 (see in Fig. 2b) and results information corresponding to the surface fractal. After the initial increasing section, there is a linear range with zero slope, which also confirms the smooth surface of MNP particles [38].

3.2. The pH-dependent charging and colloidal stability of magnetic dispersions

The changes in average hydrodynamic size ($Z\text{-Ave}$) and zeta potential of the PAM@MNP nanoparticles and PEI-clusters are plotted as a function of pH in Fig. 3a,b. A few representative samples of CB-clusters are shown in Fig. 3a to demonstrate the aggregated (photo on the left) and colloidally stable (last two photos) magnetic sols. Photos of PEI-clusters after settling for 3 h at different salt concentrations are shown in Fig. 3c.

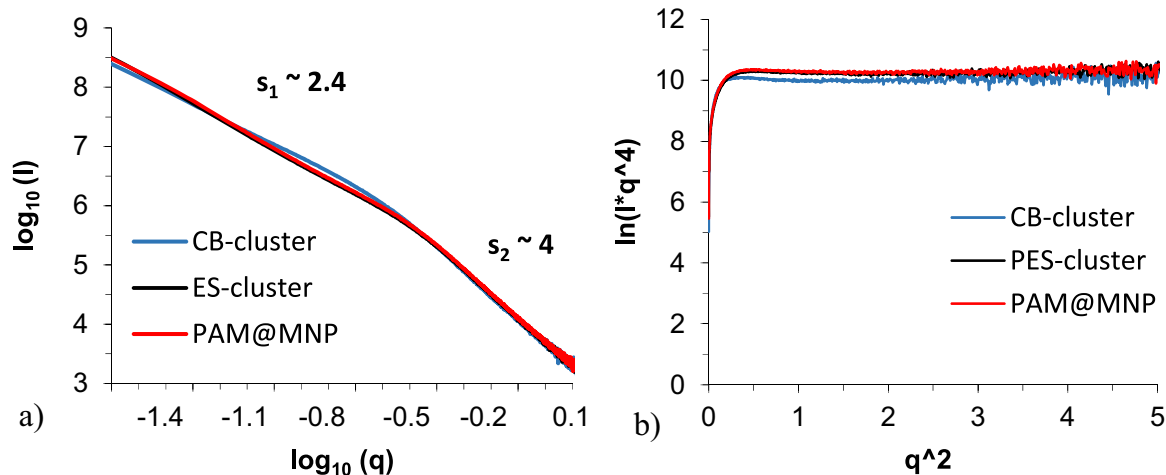


Fig. 2. SAXS results for PAM@MNP nanoparticles and PEI-clusters a) as double logarithmic plot (the opposite values of slope (s_1 , s_2) inserted on the graph are characteristic for volume fractal and the power of Porod's law ($I(q) \sim S q^{-s}$) if interface is flat, respectively) and b) as Porod plot.

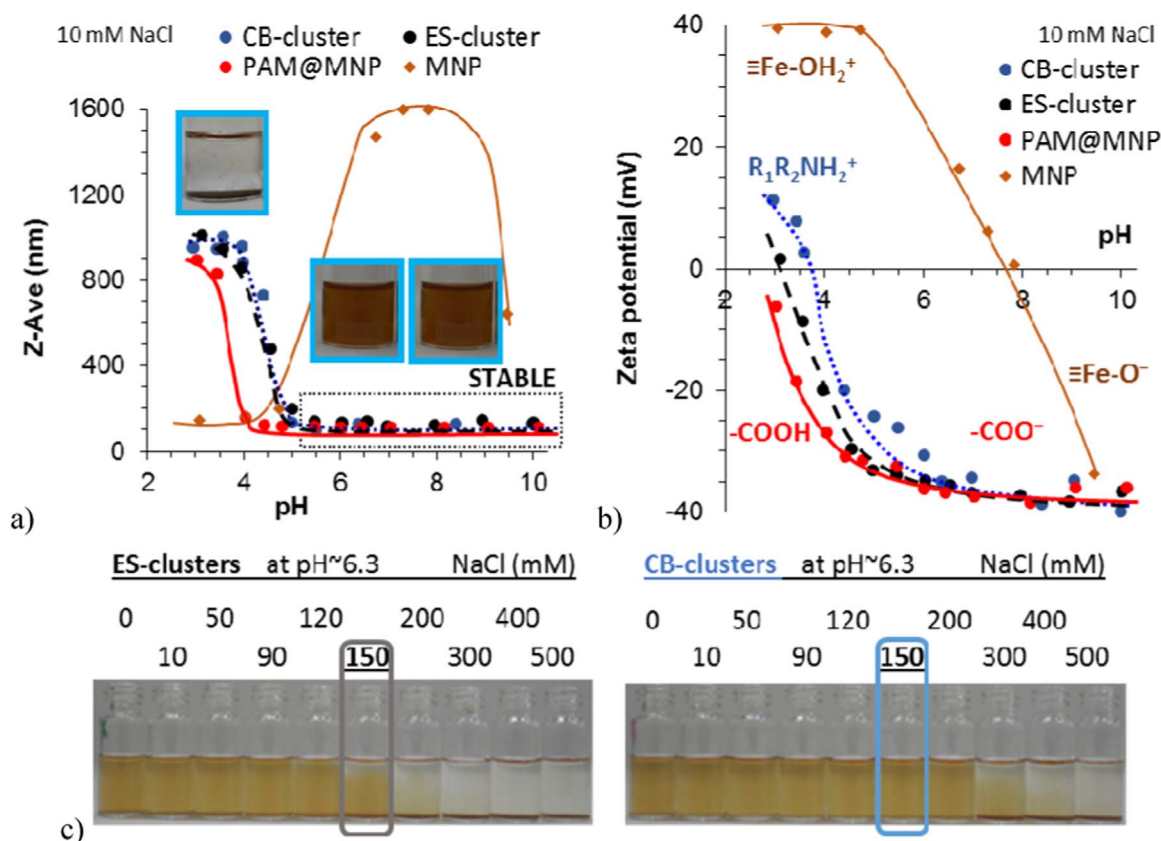


Fig. 3. pH-dependence of a) average hydrodynamic size (*Z-Ave*) and b) zeta potential of PAM@MNP nanoparticles and PEI-clusters at ionic strength of 10 mM. c) Stable and sedimented PEI-clusters in different salt solutions at pH ~6.3 (photos were taken after standstill for 3 h). The photos inserted into the figure a) demonstrate the aggregated and stable sols of CB-clusters. The results of naked MNPs [22] are recalled here for comparison.

The naked magnetite nanoparticles in aqueous media have a pH-dependent surface charging and aggregation state, namely the reactions of surface $\equiv\text{Fe}-\text{OH}$ sites lead to the formation of positive ($\equiv\text{Fe}-\text{OH}_2^+$) and negative surface ($\equiv\text{Fe}-\text{O}^-$) charges at pH values below and above ~8, respectively. For MNPs, pH~8 is characteristic, and is called the isoelectric point (*IEP*), this is where the amounts of oppositely charged surface sites are equal to each other. At pH values close to the *IEP*, the zeta potential of MNP nanoparticles is around zero, thus the MNPs are aggregated (averaged hydrodynamic size ~1600 nm) in the absence of stabilizing electrostatic forces. The physiological pH (e.g., in blood pH~7.2–7.4) is close to the *IEP*, thus the surface of naked MNPs should be modified to prevent their aggregation which is dangerous in the body [16,22].

The addition of an appropriate amount of biocompatible polyelectrolyte can electrosterically stabilize the MNP particles at the bio relevant pH-range. Here we used PAM to prepare PAM@MNP core-shell nanoparticles as it has been detailed in the Section 2.1. (Materials). The PAM adsorbs onto the MNP-surface via $-\text{COOH}/-\text{COO}^-$ groups and its unbounded negatively charged functional groups ($-\text{COO}^-$) can cause reversal of the zeta potential value (circa -40 mV). The MNPs adsorbed approximately 0.9 mmol/g PAM corresponding to the full coverage of MNPs [23,30], and they are colloidally stable (*Z-average* hydrodynamic size ~110 nm) at pH above ~4 as it is seen in Fig. 3a.

The electrokinetic potentials of the PAM@MNP nanoparticles and PEI-clusters are the same at pH above ~6, nevertheless the zeta potential values of clusters are shifted in a positive direction compared to the PAM@MNP particles at pH below ~6 (see in Fig. 3b). This confirms the interaction between PEI and PAM@MNP particles via the primary amine and carboxylate groups. The slightly higher zeta potential values at pH < 6 are likely due to the protonation of free

secondary amine groups ($\text{R}_1\text{R}_2\text{NH}_2^+$) of PEI. Because of the decrease in the absolute value of the zeta potential, the electrosteric stabilization of the PEI-clusters is less effective, which causes the increase of the *Z-average* hydrodynamic size at the same pH values. The PEI-clusters are colloidally stable at pH above ~5.5 as it is seen in Fig. 3a which still meet the requirement to be stable in the biological medium.

The ES- and CB-clusters at different salt concentrations have different settling properties as it is seen in Fig. 3c. After 3-h-sedimentation, the ES-cluster is settled and the CB-clusters remains stable even at 150 mM NaCl. The salt tolerance of CB-cluster is better and obviously exceeds the physiological value at pH~6.3.

3.3. FTIR-ATR analysis of the clustering process

Attenuated total reflection Fourier transform infrared spectroscopy analysis was used to characterize the formed bonds after the clustering process. Fig. 4a shows the IR absorption spectra of PEI, PAM@MNP nanoparticles and PEI-clusters. Fig. 4b shows the subtracted spectra of the PEI-clusters compared to PEI and the positions of characteristic bands are collected in Table 2.

In the spectra of PAM@MNP nanoparticles and PEI-clusters (see Fig. 4a) two characteristic bands of magnetite are present, i.e., the Fe–O band at ~ 550 cm^{-1} and the H-bonded OH-stretching at ~ 1630 cm^{-1} [39,40] close to a band of PEI at ~ 1620 cm^{-1} . PAM@MNP nanoparticles have characteristic bands at ~ 1720 cm^{-1} , ~ 1580 cm^{-1} and ~ 1410 cm^{-1} [23] belonging to the $-\text{COOH}/-\text{COO}^-$ moieties. In Fig. 4a the spectra of PAM@MNP nanoparticles and PEI-clusters seem to be similar, thus for the accurate evaluation of the bonds in clusters, the subtraction of spectra is essential. The spectra of PEI-cluster – PAM@MNP and the spectrum of PEI are compared in Fig. 4b.

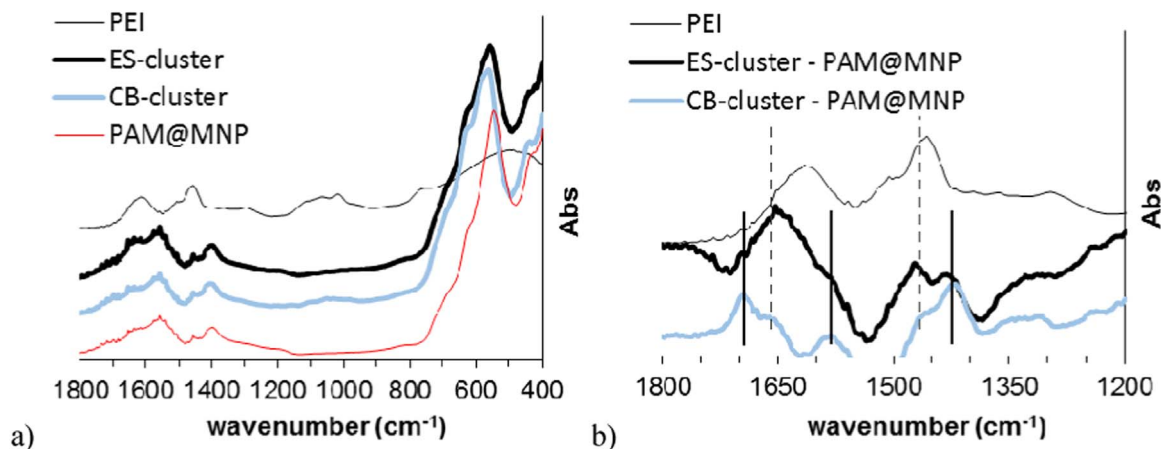


Fig. 4. a) FTIR-ATR spectra of PEI, PAM@MNP nanoparticles and PEI-clusters, b) subtracted spectra of PEI-clusters compared to the IR spectrum of PEI. Samples were dried on the diamond crystal from solution/dispersion at pH \sim 6.3. Absorbance is given in arbitrary units. Solid lines mark the position of bands related to amide bond and dashed lines indicate the bands of primary amine groups ($-\text{NH}_3^+$).

Table 2

Characteristic peaks of PEI, ES-cluster – PAM@MNP and CB-cluster – PAM@MNP spectra. The wavenumbers are given in cm^{-1} . (The sign 's' means shoulder on the spectrum.)

Measured samples			Explanation	
PEI	ES-cluster–PAM@MNP	CB-cluster–PAM@MNP	Typical band	Type of bond
–	–	1695	$\text{C}=\text{O}$ [42–44]	Amide bond
1616	1652	1652 (s)	$-\text{NH}_2$ bending [41,42]	$-\text{NH}_3^+$ in bond
–	1581 (s)	1581	CNH bending [42–44]	Amide bond
1458	1471	1467 (s)	C–N stretching [41,42]	$-\text{NH}_3^+$ in bond
–	1431	1419	C–N stretching [42–44]	Amide bond

The bands of PEI at \sim 1620 cm^{-1} and \sim 1460 cm^{-1} belong to $-\text{NH}_2$ bending and C–N stretching [41,42], respectively. In the subtracted spectrum of ES-cluster, these bands can be found at \sim 1650 cm^{-1} and \sim 1470 cm^{-1} , i.e., both peaks were shifted to the higher wavenumber region. Based on this, the $-\text{NH}_2$ moieties are involved in the clustering process and according to the adjusted pH the $-\text{NH}_3^+$ functional groups of PEI are electrostatically bonded to the free $-\text{COO}^-$ groups of PAM on PAM@MNP surface.

In the subtracted spectrum of CB-cluster, shoulders can also be seen at \sim 1650 cm^{-1} and \sim 1470 cm^{-1} , which means, analogously to the previous, that small amount of electrostatically bonded PEI is present even in these clusters. Nevertheless, there are three new intense bands in this subtracted spectrum at \sim 1695 cm^{-1} , \sim 1580 cm^{-1} and \sim 1420 cm^{-1} , assigned to $\text{C}=\text{O}$, CNH bending and C–N stretching [42–44], respectively. All these bands are characteristic of the amide bonds, which clearly prove that the $-\text{NH}_2/-\text{NH}_3^+$ groups of PEI are chemically bonded to the free $-\text{COOH}/-\text{COO}^-$ groups of PAM on the MNP nanoparticles after the clustering process. In case of ES-cluster these bands are weaker, thus only a small amount of PEI is chemically bonded in these clusters.

The FTIR-ATR analysis allowed us to obviously distinguish the electrostatically and chemically bonded PEI, and although both types of bond formation are present in both clusters, their ratios are characteristic for the two different synthesis processes.

3.4. Magnetic hyperthermia efficiency of PEI-clusters

The heating effect of electrostatically and chemically bonded PEI–

clusters was tested in concentrated magnetic fluids. The effect of AC magnetic field can be seen as the increase in the temperature of the aqueous dispersions as a function of time in Fig. 5. First the magnetic field was kept constant at $B = 9.146$ mT while the resonant frequency varied, then the resonant frequency was set constant ($f = 109.5$ kHz) and the magnetic field was different. The initial slope of the heating curves ($\Delta T/\Delta t$) were calculated in the range of 20–200 s and the calculated SAR values related to unit mass of magnetite (see in Section 2.7. (Magnetic hyperthermia)) are represented in Fig. 6a, b as a function of resonant frequency and magnetic field, respectively.

The SAR values increase with the increasing resonant frequency as well as with the increasing magnetic field. The obtained SAR values are fully consistent with others found in the literature [30,45–50]. The better magnetic heating efficiency of the CB-cluster is likely to be explained by their larger size and looser structure as determined by TEM, due to better accessibility of water molecules to magnetic cores of clusters. The heating efficiency characteristic for our clusters should be adequate to heat up the treated area with \sim 5 $^\circ\text{C}$ above the body temperature, thus an effective magnetic hyperthermia treatment is probably feasible.

Under an alternating magnetic field, local heating can be induced even in the non-magnetic living tissues which is an undesired damaging effect [51,52]. To eliminate this phenomenon, Brezovich found that the product of field strength and frequency should be limited to $4.85 \times 10^8 \text{ Am}^{-1} \text{ s}^{-1}$ [53], at the same time Hergt and Dutz suggest another criterion at $5 \times 10^9 \text{ Am}^{-1} \text{ s}^{-1}$ [54]. In case of our experiments, the maximum value of the product mentioned above is $4.5 \times 10^9 \text{ Am}^{-1} \text{ s}^{-1}$ (at 621.7 kHz and 9.146 mT) which seems to be acceptable.

3.5. MRI contrasting properties of PEI-clusters

The contrast enhancement efficiency of PAM@MNP nanoparticles and PEI-clusters prepared by electrostatic or chemical way was tested in MRI measurements. In general, the longitudinal relaxivity values ($r1$) are very small, characteristic of superparamagnetic iron oxide nanoparticles (SPION) [18] thus the $r1$ values were not worth determining for our samples. The transverse relaxivity values ($r2$) were calculated by plotting the relaxation rates ($R2 = 1/T2$) against the Fe concentration as described in our previous papers [18,19]. Enhancement of $T2$ contrast was recorded for the PEI-clusters compared to the PAM@MNP nanoparticles, shown in Fig. 7 as the concentration dependence of the $R2$ relaxation rate.

The calculated values of transverse relaxivity were extremely high ($r2 \sim 390\text{--}690 \text{ mM}^{-1} \text{ s}^{-1}$) related to the majority of data published for

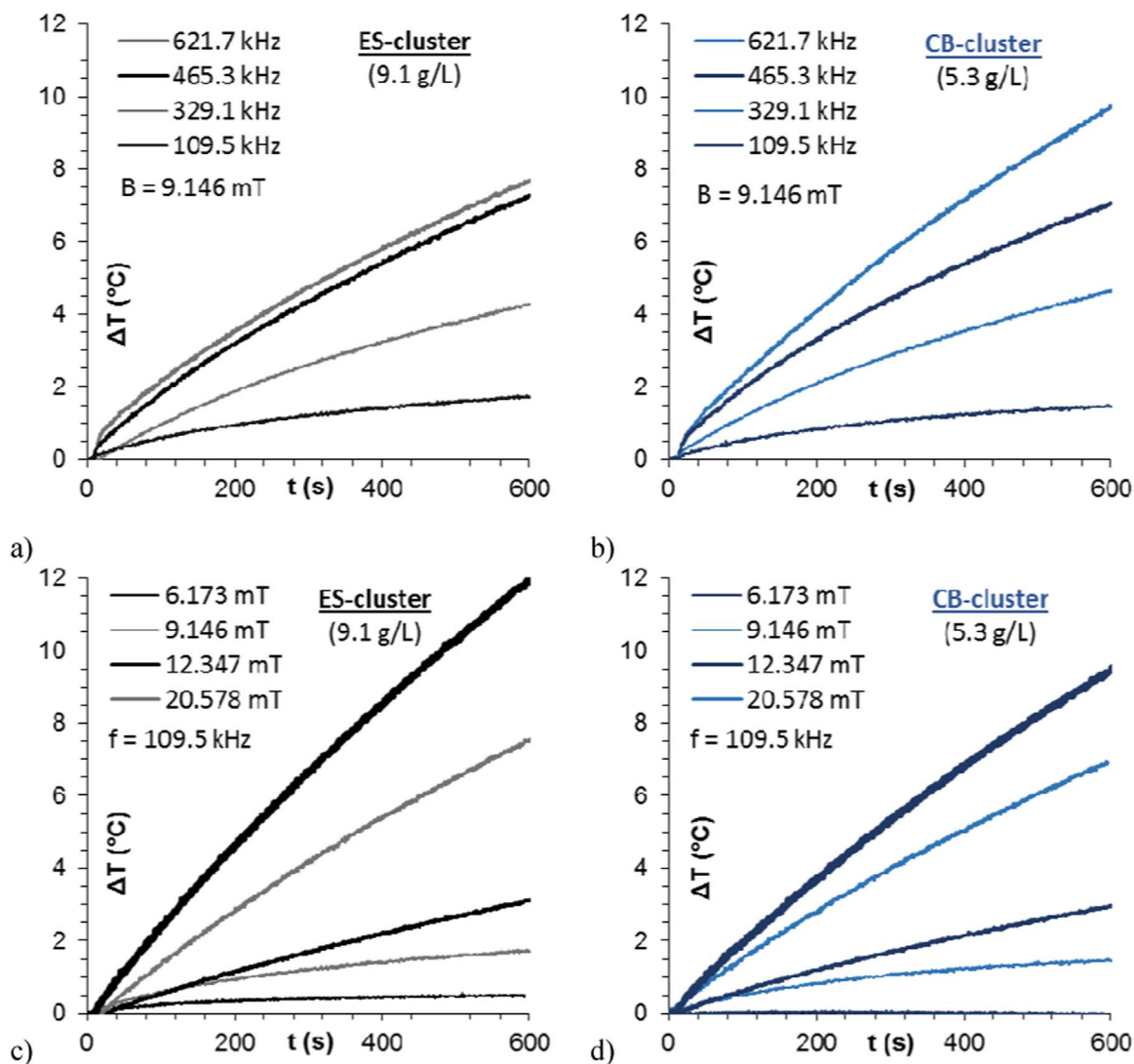


Fig. 5. The temperature change as a function of time in magnetic hyperthermia measurements of (a,c) electrostatically and (b,d) chemically bonded PEI-clusters (a,b) at a constant magnetic field ($B=9.146$ mT) with varied resonant frequencies and (c,d) at constant resonant frequency ($f=109.5$ kHz) with different magnetic fields, respectively. The initial slope of $\Delta T/\Delta t$ was calculated in the range of 20–200 s.

MNPs ($r_2 \sim 50\text{--}310$ $\text{mM}^{-1} \text{s}^{-1}$) [19,55–59]. For example Resovist has $r_2=306$ $\text{mM}^{-1} \text{s}^{-1}$, this material is generally used as reference superparamagnetic iron oxide MRI contrast agent although its FDA approval

has not yet been completed [20].

The transverse relaxivity of PAM@MNP is 389 $\text{mM}^{-1} \text{s}^{-1}$ and this is almost equal to the value characteristic for polygallate coated MNPs

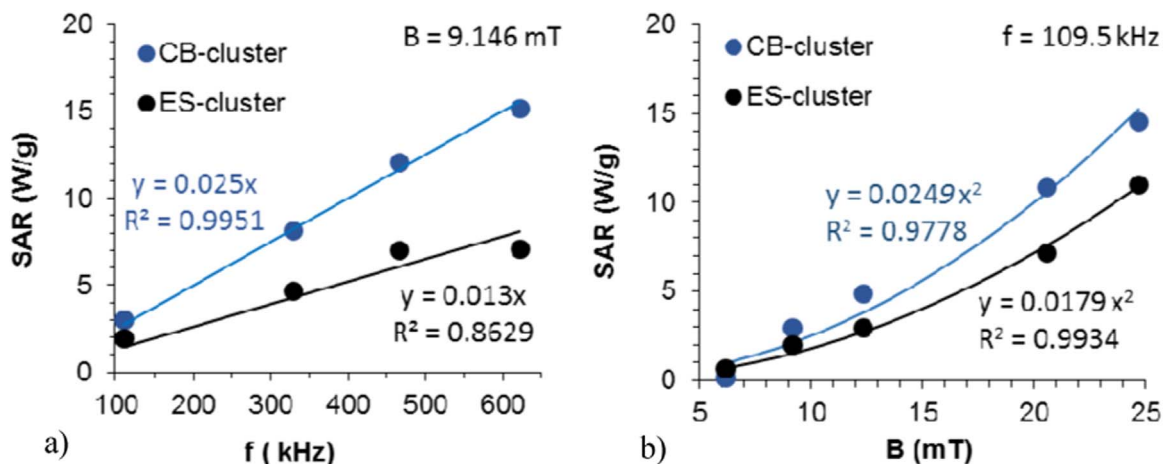


Fig. 6. The heating efficiency of electrostatically and chemically bonded PEI-clusters as a function of a) resonant frequency in $B=9.146$ mT and b) magnetic field at $f=109.5$ kHz. The SAR values are related to 1 g magnetite. The symbols represent the measured data and the lines are the results of fitting.

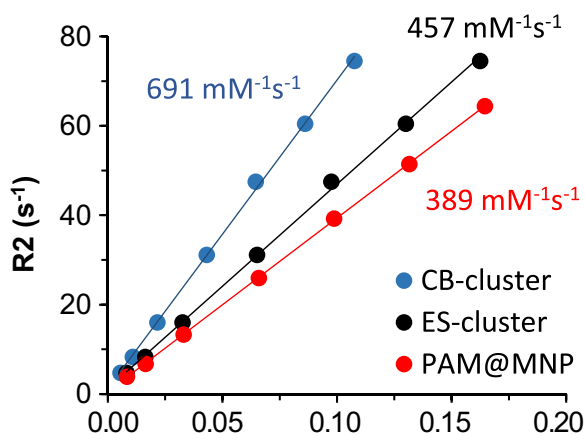


Fig. 7. Transverse relaxation rate ($R_2=1/T_2$) of the samples PAM@MNP nanoparticles and PEI-clusters prepared by electrostatic or chemical way as a function of iron concentration and the resulting r_2 relaxivity values.

(PGA@MNP, $r_2=387 \text{ mM}^{-1} \text{ s}^{-1}$) [45]. PAM is a negatively charged polyelectrolyte even like PGA, and the high transverse relaxivity is due the strong hydration of the densely charged negative shell near the MNP core. The enhanced relaxation of large amount of protons near the magnetite surface leads to an increase in the contrast. The r_2 relaxivity of the PAM@MNP dispersion is somewhat lower than that of naked MNPs (measured at pH ~ 4 as $430 \text{ mM}^{-1} \text{ s}^{-1}$ [19]) but at the same time the PAM@MNP is biocompatible under physiological conditions [23].

The magnetic nanoparticles with a potential feasibility in MRI applications are typically in the so called “motional averaging regime” (MAR). In this regime the transverse relaxivity of magnetic agglomerates first increases with their size [18,25], and after reaching a maximum the r_2 value begins to decrease [25]. The r_2 relaxivities of ES- and CB-clusters are $457 \text{ mM}^{-1} \text{ s}^{-1}$ and $691 \text{ mM}^{-1} \text{ s}^{-1}$, respectively. These values are significantly higher than the $r_2=389 \text{ mM}^{-1} \text{ s}^{-1}$ typical for PAM@MNP nanoparticles which can be explained by the increased size of clusters. The chemically bonded cluster has about one and a half times better contrast enhancement effect compared with the electrostatically bonded PEI-cluster. The structure of ES-clusters is more compact as determined by TEM and SAXS as well. Thus the water accessibility to MNPs is lower in this sample, which reduces its efficiency in MRI [60]. The extreme high contrast enhancement effect for CB-cluster is very promising in terms of biomedical application in future.

4. Conclusion

PEI-clusters were prepared via electrostatic and chemical route and they were characterized comprehensively. The clusters were characterized by TEM, showing that the average area occupied by the chemically bonded clusters on grid was about twice as large as that of ES-cluster samples moreover the CB-clusters were more opened so less compact than ES-clusters. Based on the SAXS results, the formation of PEI-cluster has no significant effect on the scattering behavior of the systems, the surface of nanoparticles was smooth and the MNP particles were relatively close packed. The PEI-clusters show pH-dependent aggregation state and zeta potential, the chemically bonded clusters were colloidally stable at pH > 5 and even in 150 mM NaCl solution at pH ~ 6.3 , which is still relevant to the biological medium. The analysis of ATR-FTIR spectra proves that different bonds (electrostatic adhesion between $-\text{NH}_3^+$ and $-\text{COO}^-$ or amide bond, respectively) form between PAM@MNP and PEI in the electrostatic and chemical synthesis routes. Magnetic hyperthermia studies showed that the values of specific absorption rate (SAR) are about two times larger in case of the CB-cluster than that of ES-cluster. Besides that the MRI

experiments proved exceptionally high transversal relaxivities for both types of MNP clusters, it was shown that the r_2 value of CB-cluster is definitely greater than that characteristic of PAM@MNP and ES-cluster. Based on these results, the chemically clustered product shows greater potential for feasible theranostic applications.

Acknowledgements

This research was supported by OTKA (NK 84014) grant and RADIOMAG (COST action TD1402). The authors are grateful to Vasily Haramus (Helmholtz-Zentrum Geesthacht, Zentrum für Material- und Küstenforschung, Geesthacht, Germany), Rodica Turcu (National Institute R & D of Isotopic and Molecular Technologies, Cluj-Napoca, Romania) and Laszlo Vekas (Center for Fundamental and Advanced Technical Research, Romanian Academy Timișoara-Branch, Timișoara, Romania) for the SAXS measurements and to Daniel Sebők (Department of Physical Chemistry and Materials Sciences, University of Szeged, Szeged, Hungary) for his help in the analysis of SAXS results.

References

- [1] A.K. Gupta, M. Gupta, Synthesis and surface engineering of iron oxide nanoparticles for biomedical applications, *Biomaterials* 26 (2005) 3995–4021.
- [2] W. Andr, U.H. Hafeli, R. Hergt, R. Misri, Application of magnetic particles in medicine and biology, in: H. Kronmüller, S. Parkin (Eds.), *Handbook of Magnetism and Advanced Magnetic Materials*, John Wiley & Sons Ltd, New York, 2007.
- [3] E. Munnier, S. Cohen-Jonathan, C. Linossier, L. Douzich-Eyrolles, H. Marchais, M. Soucé, K. Hervé, P. Dubois, I. Chourpa, Novel method of doxorubicin–SPION reversible association for magnetic drug targeting, *Int. J. Pharm.* 363 (2008) 170–176.
- [4] S. Laurent, D. Forge, M. Port, A. Roch, C. Robic, L. Vander Elst, R.N. Muller, Magnetic iron oxide nanoparticles: synthesis, stabilization, vectorization, physico-chemical characterizations, and biological applications, *Chem. Rev.* 108 (2008) 2064–2110.
- [5] Q.A. Pankhurst, N.K.T. Thanh, S.K. Jones, J. Dobson, Progress in applications of magnetic nanoparticles in biomedicine, *J. Phys. D Appl. Phys.* 42 (2009) 224001–224015.
- [6] C. Boyer, M.R. Whittaker, V. Bulmus, J. Liu, T.P. Davis, The design and utility of polymer-stabilized iron-oxide nanoparticles for nanomedicine applications, *NPG Asia Mater.* 2 (2010) 23–30.
- [7] E. Amstad, M. Textora, E. Reimhult, Stabilization and functionalization of iron oxide nanoparticles for biomedical applications, *Nanoscale* 3 (2011) 2819–2843.
- [8] J.K. Oh, J.M. Park, Iron oxide-based superparamagnetic polymeric nanomaterials: design, preparation, and biomedical application, *Prog. Polym. Sci.* 36 (2011) 168–189.
- [9] L.H. Reddy, J.L. Arias, J. Nicolas, P. Couvreur, Magnetic nanoparticles: design and characterization, toxicity and biocompatibility, pharmaceutical and biomedical applications, *Chem. Rev.* 112 (2012) 5818–5878.
- [10] M. Colombo, S. Carregal-Romero, M.F. Casula, L. Gutiérrez, M.P. Morales, I.B. Böhm, J.T. Heverhagen, D. Prosser, W.J. Parak, Biological applications of magnetic nanoparticles, *Chem. Soc. Rev.* 41 (2012) 4306–4334.
- [11] G. Kandasamy, D. Maity, Recent advances in superparamagnetic iron oxide nanoparticles (SPIOs) for in vitro and in vivo cancer nanotheranostics, *Int. J. Pharm.* 496 (2015) 191–218.
- [12] T.K. Jain, J. Richey, M. Strand, D.L. Leslie-Pelecky, C.A. Flask, V. Labhasetwar, Magnetic nanoparticles with dual functional properties: drug delivery and magnetic resonance imaging, *Biomaterials* (29) (2008) 4012–4021.
- [13] V.I. Shubayev, T.R. Pisanic, S. Jin, Magnetic nanoparticles for theranostics, *Adv. Drug Deliv. Rev.* 61 (2009) 467–477.
- [14] O. Veisheh, J.W. Gunn, M. Zhang, Design and fabrication of magnetic nanoparticles for targeted drug delivery and imaging, *Adv. Drug Deliv. Rev.* 62 (2010) 284–304.
- [15] N. Fautcon, A. Bée, J. Roger, J.N. Pons, Synthesis of aqueous magnetic liquids by surface complexation of maghemite nanoparticles, *J. Mol. Liq.* 83 (1999) 233–242.
- [16] Q.A. Pankhurst, J. Connolly, S.K. Jones, J. Dobson, Applications of magnetic nanoparticles in biomedicine, *J. Phys. D: Appl. Phys.* 36 (2003) R167–R181.
- [17] E. Illés, E. Tombácz, The effect of humic acid adsorption on pH-dependent surface charging and aggregation of magnetite nanoparticles, *J. Colloid Interf. Sci.* 295 (2006) 115–123.
- [18] E. Illés, M. Szekeres, E. Kupcsik, I.Y. Tóth, K. Farkas, A. Jedlovsky-Hajdú, E. Tombácz, PEGylation of surfacted magnetite core-shell nanoparticles for biomedical application, *Colloid Surf. A* 460 (2014) 429–440.
- [19] A. Jedlovsky-Hajdú, E. Tombácz, I. Bányai, M. Babos, A. Palkó, Carboxylated magnetic nanoparticles as MRI contrast agents: relaxation measurements at different field strengths, *J. Magn. Magn. Mater.* 324 (2012) 3173–3180.
- [20] M. Szekeres, I.Y. Tóth, E. Illés, A. Hajdú, I. Zupkó, K. Farkas, G. Oszlányi, L. Tiszlavicz, E. Tombácz, Chemical and colloidal stability of carboxylated core-shell magnetite nanoparticles designed for biomedical applications, *Int. J. Mol. Sci.*

- 14 (2013) 14550–14574.
- [21] A. Hajdu, M. Szekeres, I.Y. Tóth, R.A. Bauer, J. Mihaly, I. Zupko, E. Tombacz, Enhanced stability of polyacrylate-coated magnetite nanoparticles in biorelevant media, *Colloid Surf. B Biointerfaces* 94 (2012) 242–249.
- [22] I.Y. Tóth, E. Illés, M. Szekeres, E. Tombacz, Preparation and characterization of chondroitin-sulfate-a coated magnetite nanoparticles for biomedical applications, *J. Magn. Magn. Mater.* 380 (2015) 168–174.
- [23] I.Y. Tóth, E. Illés, R.A. Bauer, D. Nesztor, M. Szekeres, I. Zupkó, E. Tombacz, Designed polyelectrolyte shell on magnetite nanocore for dilution-resistant biocompatible magnetic fluids, *Langmuir* 28 (2012) 16638–16646.
- [24] R.P. Friedrich, J. Zaloga, E. Schreiber, I.Y. Tóth, E. Tombacz, S. Lyer, C. Alexiou, Tissue plasminogen activator binding to superparamagnetic iron oxide nanoparticle – covalent versus adsorptive approach, *Nanoscale Res. Lett.* 11 (2016) 297.
- [25] N. Lee, T. Hyeon, Designed synthesis of uniformly sized iron oxide nanoparticles for efficient magnetic resonance imaging contrast agents, *Chem. Soc. Rev.* 41 8 (2012) 2575–2589.
- [26] B.L. Frankamp, A.K. Boal, M.T. Tuominen, V.M. Rotello, Direct control of the magnetic interaction between iron oxide nanoparticles through dendrimer-mediated self-assembly, *J. Am. Chem. Soc.* 127 (2005) 9731–9735.
- [27] J.L. Dormann, D. Fiorani, E. Tronc, Magnetic relaxation in fine-particle systems, *Adv. Chem. Phys.* 98 (1997) 283–494.
- [28] Z. Lu, Y. Yin, Colloidal nanoparticle clusters: functional materials by design, *Chem. Soc. Rev.* 41 (2012) 6874–6887.
- [29] J.F. Berret, N. Schonbeck, F. Gazeau, D. El Kharrat, O. Sandre, A. Vacher, M. Airiau, Controlled clustering of superparamagnetic nanoparticles using block copolymers: design of new contrast agents for magnetic resonance imaging, *J. Am. Chem. Soc.* 128 (2006) 1755–1761.
- [30] D. Nesztor, K. Bali, I.Y. Tóth, M. Szekeres, E. Tombacz, Controlled clustering of carboxylated SPIONs through polyethylenimine, *J. Magn. Magn. Mater.* 380 (2015) 144–149.
- [31] E. Tombacz, E. Illés, A. Majzik, A. Hajdú, N. Rídeg, M. Szekeres, Ageing in the inorganic nanoworld: example of magnetite nanoparticles in aqueous medium, *Croat. Chem. Acta* 80 (2007) 503–515.
- [32] I.Y. Tóth, M. Szekeres, R. Turcu, S. Sáring, E. Illés, D. Nesztor, E. Tombacz, Mechanism of in-situ surface polymerization of gallic acid in an environmental-inspired preparation of carboxylated core-shell magnetite nanoparticles, *Langmuir* 30 (2014) 15451–15461.
- [33] I. Szilágyi, D. Rosická, J. Hierrezuelo, M. Borkovec, Charging and stability of anionic latex particles in the presence of linear poly (ethylene imine), *J. Colloid Interf. Sci.* 360 (2) (2011) 580–585.
- [34] M. Finessi, P. Sinha, I. Szilágyi, I. Popa, P. Maroni, M. Borkovec, Charge reversal of sulfate latex particles by adsorbed linear poly (ethylene imine) probed by multi-particle colloidal probe technique, *J. Phys. Chem. B.* 115 (29) (2011) 9098–9105.
- [35] G.T. Hermanson, *Bioconjugate Techniques, Chapter 3: Zero-length crosslinkers*, Academic Press, New York, 2008.
- [36] T. Gorniak, T. Haraszti, V.M. Garamus, A.R. Buck, T. Senkbeil, M. Priebe, A. Hedberg-Buenz, D. Koehn, T. Salditt, M. Grunze, M.G. Anderson, A. Rosenhahn, Nano-scale morphology of melanosomes revealed by small-angle X-ray scattering, *PLoS ONE* 9 (2014) e90884.
- [37] R. Turcu, I. Craciunescu, V.M. Garamus, C. Janko, S. Lyer, R. Tietze, C. Alexiou, L. Vekas, Magnetic microgels for drug targeting applications: physical–chemical properties and cytotoxicity evaluation, *J. Magn. Magn. Mater.* 380 (2015) 307–314.
- [38] L. Zhi-Hong, A program for SAXS data processing and analysis, *Chin. Phys.* 37 (2013) 108002.
- [39] G.S.R. Krishnamurti, P.M. Huang, Influence of citrate on the kinetics of Fe(II) oxidation and the formation of iron oxyhydroxides, *Clay. Clay. Miner.* 39 (1991) 28–34.
- [40] Y.S. Li, J.S. Church, A.L. Woodhead, Infrared and Raman spectroscopic studies on iron oxide magnetic nano-particles and their surface modifications, *J. Magn. Magn. Mater.* 324 (2012) 1543–1550.
- [41] M. Seitz, J.Y. Wong, C.K. Park, N.A. Alcantar, J. Israelachvili, Formation of tethered supported bilayers via membrane-inserting reactive lipids, *Thin Solid Films* 327–329 (1998) 767–771.
- [42] P. Larkin, *Infrared and Raman Spectroscopy, Principles and Spectral Interpretation*, Elsevier, USA, 2011.
- [43] H. Fabian, W. Mäntele, Infrared spectroscopy of proteins, in: J.M. Chalmers, P.R. Griffiths (Eds.), *Handbook of Vibrational Spectroscopy, Applications in Life, Pharmaceutical and Natural Sciences* 5, John Wiley & Sons Ltd, New York, 2002.
- [44] L.K. Tamm, S.A. Tatulian, Infrared spectroscopy of proteins and peptides in lipid bilayers, *Q. Rev. Biophys.* 30 (1997) 365–429.
- [45] M. Szekeres, E. Illés, C. Janko, K. Farkas, I.Y. Tóth, D. Nesztor, I. Zupkó, I. Földes, C. Alexiou, E. Tombacz, Hemocompatibility and biomedical potential of Poly(gallic acid) coated iron oxide. Nanoparticles for theranostic use, *J. Nanomed. Nanotech* 6 (2015) 252.
- [46] A. Cervadoro, C. Giverso, R. Pande, S. Sarangi, L. Preziosi, J. Wosik, A. Brazdeikis, P. Decuzzi, Design maps for the hyperthermic treatment of tumors with superparamagnetic nanoparticles, *PLoS One* 8 (2013) e57332.
- [47] E. Cheraghpour, S. Javadpour, A.R. Mehdizadeh, Citrate capped superparamagnetic iron oxide nanoparticles used for hyperthermia therapy, *J. Biomed. Sci. Eng.* 5 (2012) 715–719.
- [48] J. Motoyama, T. Hakata, R. Kato, N. Yamashita, T. Morino, T. Kobayashi, H. Honda, Size dependent heat generation of magnetite nanoparticles under AC magnetic field for cancer therapy, *Biomagn. Res. Technol.* 6 (2008) 4.
- [49] J.P. Bullivant, B. Zhao, B.J. Willenberg, B. Kozissnik, C.D. Batich, J. Dobson, Materials characterization of Feraheme/Ferumoxyl and preliminary evaluation of its potential for magnetic fluid hyperthermia, *Int. J. Mol. Sci.* 14 (2013) 17501–17510.
- [50] C. Grüttner, K. Müller, J. Teller, F. Westphal, Synthesis and functionalisation of magnetic nanoparticles for hyperthermia applications, *Int. J. Hyperther.* 29 (2013) 777–789.
- [51] A.E. Deatsch, B.A. Evans, Heating efficiency in magnetic nanoparticle hyperthermia, *J. Magn. Magn. Mater.* 354 (2014) 163–172.
- [52] I.M. Obaidat, B. Issa, Y. Haik, Magnetic properties of magnetic nanoparticles for efficient hyperthermia, *Nanomaterials* 5 (2015) 63–89.
- [53] I.A. Brezovich, Low frequency hyperthermia: capacitive and ferromagnetic thermoseed methods, *Med. Phys. Monogr.* 16 (1988) 82–11.
- [54] R. Hergt, S. Dutz, Magnetic particle hyperthermia – biophysical limitations of a visionary tumor therapy, *J. Magn. Magn. Mater.* 3011 (2007) 187–192.
- [55] H. Gupta, P. Paul, N. Kumar, S. Baxi, D.P. Das, One pot synthesis of water-dispersible dehydroascorbic acid coated Fe₃O₄ nanoparticles under atmospheric air: blood cell compatibility and enhanced magnetic resonance imaging, *J. Colloid Interf. Sci.* 430 (2014) 221–228.
- [56] N. Arsalani, H. Fattahi, M. Nazarpour, Synthesis and characterization of PVP functionalized superparamagnetic Fe₃O₄ nanoparticles as an MRI contrast agent, *Express Polym. Lett.* 4 (2010) 329–338.
- [57] U.I. Tromsdorf, O.T. Bruns, S.C. Salmen, U. Beisiegel, H. Weller, A highly effective, nontoxic T1 MR contrast agent based on ultrasmall PEGylated iron oxide nanoparticles, *Nano Lett.* 9 (2009) 4434–4440.
- [58] J. Huang, X. Zhong, L. Wang, L. Yang, H. Mao, Improving the magnetic resonance imaging contrast and detection methods with engineered magnetic nanoparticles, *Theranostics* 2 (2012) 86–102.
- [59] M. Shao, C. Min, D. Issadore, M. Liang, T.J. Yoon, R. Weissleder, H. Lee, Magnetic nanoparticles and microNMR for diagnostic applications, *Theranostics* 2 (2012) 55–65.
- [60] A.Z. Abbasi, L. Gutiérrez, L.L. del Mercato, F. Herranz, O. Chubykalo-Fesenko, S. Veintemillas-Verdaguer, W.J. Parak, M.P. Morales, J.M. González, A. Hernando, P. de la Presa, Magnetic capsules for NMR imaging: effect of magnetic nanoparticles spatial distribution and aggregation, *J. Phys. Chem. C.* 115 (14) (2011) 6257–6264.